Title
The Halo Model of Large Scale Structure for Warm Dark Matter

Authors
Dunstan, Robyn M
Abazajian, Kevork N
Polisensky, Emil
et al.

Publication Date
2011-09-28

Peer reviewed

The Halo Model of Large Scale Structure for Warm Dark Matter

Robyn M. Dunstan[1],* Kevork N. Abazajian[1,2],† Emil Polisensky[3],‡ and Massimo Ricotti[4§]
[1]*Maryland Center for Fundamental Physics & Joint Space-Science Institute, Department of Physics, University of Maryland, College Park, Maryland 20742 USA*
[2]*Department of Physics & Astronomy, University of California, Irvine, CA 92697 USA*
[3]*Naval Research Laboratory, Washington, D.C. 20375, USA and*
[4]*Department of Astronomy, University of Maryland, College Park, Maryland 20742 USA*
(Dated: September 29, 2011)

We present a comprehensive analysis of the halo model of cosmological large to small-scale structure statistics in the case of warm dark matter (WDM) structure formation scenarios. We include the effects of WDM on the linear matter power spectrum, halo density profile, halo concentration relation, halo mass function, subhalo density profile, subhalo mass function and biasing of the smooth dark matter component. As expected, we find large differences at the smallest physical scales in the nonlinear matter power spectrum predicted in the halo model between WDM and cold dark matter even for reasonably high-scale WDM particle masses. We find that significant effects are contributed from the alteration of the halo density profile and concentration, as well as the halo mass function. We further find that the effects of WDM on the subhalo population are important but sub-dominant. Clustering effects of the biasing of the smooth component in WDM is not largely significant.

PACS numbers: 98.65.-r,95.35.+d,14.60.Pq,14.60.St

I. INTRODUCTION

The theory of large scale structure growth and formation from Gaussian, adiabatic initial conditions is in remarkable agreement with observed large scale structure in the universe at scales above the Galactic scale. With the success of the Wilkinson Microwave Anisotropy Probe [1] at determining the amplitude and shape of the matter power spectrum, and upcoming results from the Planck Probe, the primordial linear clustering of matter will be known to better than 1.1% in the amplitude and 0.22% in the slope of the power spectrum. When combined with galaxy surveys such as the Sloan Digital Sky Survey (SDSS) and 2-degree Field, the precision can be even further enhanced [2]. These precise determinations of the clustering power spectrum, coupled with the ansatz of *cold* dark matter (CDM) with a primordial power law spectrum leads to a precise prediction for the power spectrum to arbitrary small scales of relevance to galaxy formation.

However, the small-scale clustering of dark matter can be largely different at the small scales inaccessible to CMB measurements as well as galaxy surveys, yet are significant in the role of galaxy formation. The small-scale clustering of matter can be suppressed by thermal motion of the dark matter, i.e., *warm* dark matter (WDM), allowing the dark matter to free stream out of primordial potential wells. It can also be altered in extended inflationary models [3], and in the case of charged or neutral decaying [4] dark matter progenitor particles.

The suppression of power on small-scales has been proposed as a solution to a number of problems in galaxy formation: first, the reduction of satellite galaxy halos [5], second, the reduction of galaxies in voids [6, 7], third, the low concentrations of dark matter in galaxies [8], fourth, the angular momentum problem of galaxy formation [9], fifth, the formation of disk-dominated galaxies [10].

The discovery of a number of dwarf galaxies with the SDSS, and their confirmation as harboring massive dark matter halos [11], alleviates the first problem, and even more, constrains the excessive suppression present in WDM models [12]. In addition, the small-scale power spectrum of dark matter inferred from the Lyman-α forest toward distant quasars is consistent with CDM down to sub-dwarf galaxy scales [13], though the thermal history of the intergalactic medium consistent with these findings is difficult to reconcile with other measures [14]. Overall, however, there is considerable interest in WDM as a potential structure formation scenario, and as a method to test the CDM ansatz.

In this paper, we construct a complete analytic model for the clustering of dark matter in two-point statistical measures based on the halo model of large scale structure. For a review of the halo model, see Ref. [15]. The forms developed here may be extended to higher order statistics as well. The halo model has been shown to be an effective and accurate model of dark matter clustering built upon analytic and numerical structure formation statistics. And, it can be extended to models of galaxy [16], gas [17] and galaxy velocity statistics [18].

* rdunstan@umd.edu
† kevork@uci.edu
‡ Emil.Polisensky@nrl.navy.mil
§ ricotti@astro.umd.edu

It has been shown to be consistent with broad classes of galaxy clustering measures over a wide range of redshifts, c.f. Ref. [19].

The halo model has been employed to investigate the effect of baryons [20] and massive active neutrinos [21] on weak lensing statistics. Recently, the effects of WDM in weak lensing has been studied through estimates of WDM's alterations of limited components of the halo model. In Ref. [22], the effects of WDM suppression of the linear power spectrum and a suppression of the small-mass slope of the halo mass function were incorporated into an estimate of the sensitivity of future weak lensing surveys to WDM. In Ref. [23], the WDM effects of the lack of small-mass halos in the mass function, potential cores in the halo density profile, and biasing of the smooth component were also included in estimates of the sensitivity to WDM in weak lensing surveys.

In this paper, we incorporate results from our numerical simulations of WDM structure formation as well as the leading results from CDM halo statistics to construct a complete halo model of large scale structure in the case of WDM. We include new numerical simulations' measures of the halo mass function, halo profile, and sub-halo mass function in this work. Importantly, since WDM is known to strongly affect halo substructure, we include the effects of halo substructure suppression here, which has not been included in prior work. We also incorporate the change of the halo-profile density slope and the halo-profile concentration relation, which are known to depend on the initial matter power spectrum [24, 25], as well an estimate of the biasing of the smooth dark matter component in WDM similar to that in Ref. [23]. Notably, we do not include cored halos in the case of WDM since these have not been observed in our simulations or others, nor are significant cores expected from analytic Gaussian-peak statistics methods [26, 27].

Two primary candidates for WDM particles are gravitinos [28] and sterile neutrinos [29]. For concreteness, we employ the popular Dodelson-Widrow (DW) [29] thermally-produced sterile neutrino dark matter as our WDM particle dark matter candidate. All particle dark matter masses to which we refer are that of the DW sterile neutrino, unless stated otherwise.

II. SIMULATIONS

We employ three sets of simulations using cosmological parameters consistent with the third year WMAP release [30], spectral index $n = 0.951$, matter density $\Omega_m = 0.238$, baryon density $\Omega_b = 0.04$, neutrino density $\Omega_\nu = 0$, Hubble parameter $h = 0.73$, and mass fluctuation with $R = 8h^{-1}$ Mpc, $\sigma_8 = 0.751$. We assume all matter in the simulations is dark matter only but we use Ω_b for calculating the effects of baryons on the matter power spectrum. The simulations are conducted with the N-body code GADGET-2 [31] with initial conditions generated with the GRAFIC2 software package [32]. Our initial conditions include particle velocities due to the gravitational potential using the Zeldovich approximation but we do not add random thermal velocities appropriate for WDM to the simulation particles. Gravitationally bound dark matter halos are identified using the AMIGA's Halo Finder software [33]. Each simulation set consists of a single realization of the density field but with varied power spectra of fluctuations appropriate for cold dark matter (CDM) and WDM cosmologies. We use the WDM transfer function in Ref. [7] valid for gravitino particles. In Ref. [34] the transfer function of DW sterile neutrinos is shown to be nearly identical to that for gravitinos but with a scaling relationship between the particles masses. We characterize our WDM simulations in terms of the DW sterile neutrino mass.

To investigate the halo mass function our first simulation set consists of 512^3 particles in a 60^3 Mpc^3 comoving box with mass resolution $5.7 \times 10^7 M_\odot$ and force resolution 1.2 kpc. We run simulations for CDM and WDM cosmologies with sterile neutrino particle masses of 0.2, 0.7, 1.7, and 4.4 keV.

We use the high resolution simulations described in Ref. [12] to investigate the subhalo mass function. These simulations use a 'zoom' technique to sample small volumes with fine mass resolution containing two Milky Way-sized halos, M $\sim 2 \times 10^{12} M_\odot$, embedded in coarsely sampled larger volumes. The coarse volume is a 90^3 Mpc^3 comoving box with $\sim 510^3$ particles with mass and force resolutions $9.2 \times 10^4 M_\odot$ and 275 pc in the refinement region. These simulations include CDM and 4.4, 11, and 28 keV sterile-neutrino particle mass WDM cosmologies.

The purpose of our final simulation set is to investigate the halo density profile. No differences were observed in the density profile slopes of the Milky Way-sized halos simulations, however these halos are well above the scale of power suppression in the WDM cosmologies. To reduce the halo mass to $\sim 10^8 M_\odot$ we selected one of these halos for resimulation in a smaller box, 4.5^3 Mpc^3, with $\sim 255^3$ particles with mass and force resolutions of $92 M_\odot$ and 14 pc in the refinement region. We perform simulations for CDM and 28, 48, and 70 keV standard sterile-neutrino particle WDM cosmologies. We examine the halo density profiles at redshift 1.08 where the halo appears to be well relaxed in all cosmologies.

III. MATTER POWER SPECTRUM

A. Cold Dark Matter

The cold dark matter (CDM) power spectrum has been well-defined in the halo model of large scale structure (e.g., Ref. [15]). The dimensionless power spectrum is

$$\Delta^2(k) \equiv \frac{k^3 P(k)}{2\pi^2}, \tag{3.1}$$

and the mass variance within region R is $\sigma^2(R)$,

$$\sigma^2(R) = \int \frac{dk}{k} \Delta^2(k)\, \hat{W}^2(kR)\,, \tag{3.2}$$

where $\hat{W}(kR)$ is the Fourier transform of the top-hat function with radius R. The quantity σ is also given in terms of the halo mass given the mass enclosed in radius R for the mean density of the universe.

We take the linear matter power spectrum for cold dark matter from Ref. [35]. The power spectrum is the primordial power spectrum modified by the appropriate transfer function,

$$\Delta^2(k,z) = \delta_{\rm H}^2 \left(\frac{ck}{H_0}\right)^{3+n} T^2(k,z)\,, \tag{3.3}$$

where $T(k,z)$ is the CDM transfer function, δ_H is the amplitude of perturbations on the scale of today's horizon (and is absorbed into the normalization constant), and n is the initial power spectrum index. We employ the transfer function for CDM plus baryons from Ref. [35]. This transfer function is sufficiently accurate for our purposes. The cosmological parameters we use for the transfer functions and analytic halo model are: spectral index $n = 1$, CMB temperature $T_{\rm CMB} = 2.726$, dark matter density $\Omega_{\rm dm} = 0.23$, baryon density $\Omega_{\rm b} = 0.04$, neutrino density $\Omega_\nu = 0$, Hubble parameter $h = 0.7$, and mass fluctuation with $R = 8\ h^{-1}$ Mpc, $\sigma_8 = 0.8$, which are consistent with WMAP7 [1]. We explore results at redshift $z = 0$.

B. Warm Dark Matter

For the WDM case, for concreteness, we use the sterile neutrino transfer function from Ref. [36]. There is a simple scaling relation to connect between sterile neutrinos and gravitino WDM transfer functions given in Ref. [36]. The sterile neutrinos have an initial velocity dispersion, which allows them to escape the gravitational well of the small scale perturbations upon entering the horizon. This suppresses the linear matter power spectrum for small scales (large k), as shown in Fig. 1. The scale and magnitude of the suppression increases with velocity and, therefore, decreases with the mass of the sterile neutrino. The linear matter power spectrum for the suppressed sterile neutrino case at small scales is related to that in CDM by:

$$T_{\rm s}(k) \equiv \sqrt{\frac{P_{\rm sterile}(k)}{P_{\rm CDM}(k)}}. \tag{3.4}$$

In Ref. [36], the linear matter power spectrum for sterile neutrinos was calculated using CAMB [1] using a non-thermal momentum distribution and the evolution equations for massive neutrinos. The resulting fit to the sterile neutrino transfer function is

$$T_{\rm s}(k) = \left(1 + (\alpha k)^\nu\right)^{-\mu}\,, \tag{3.5}$$

where $\nu = 2.52$, $\mu = 3.08$, and α is a function of the sterile neutrino mass,

$$\alpha = a \left(\frac{m_{\rm s}}{1\,{\rm keV}}\right)^b \left(\frac{\Omega_{\rm dm}}{0.26}\right)^c \left(\frac{h}{0.7}\right)^d h^{-1}\,{\rm Mpc}, \tag{3.6}$$

where $a = 0.188$, $b = -0.858$, $c = -0.136$, and $d = 0.692$.

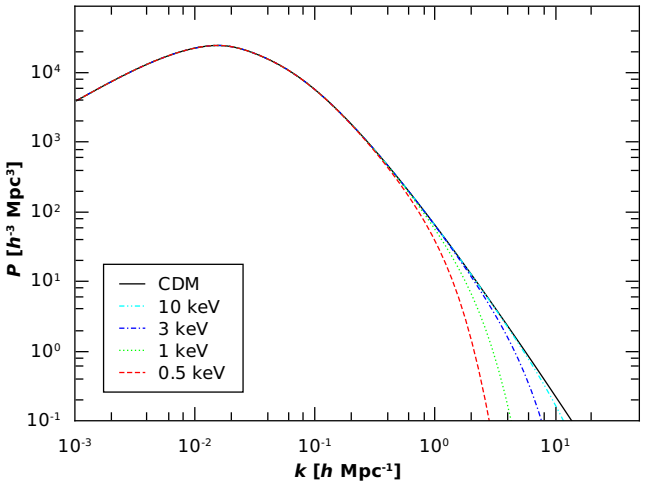

FIG. 1. Shown is the linear matter power spectrum as a function of wavenumber for the CDM model and several WDM particle masses, as listed in the legend. The smaller the WDM particle mass, the greater the suppression of the power spectrum on small scales (large k).

C. Nonlinear Matter Power Spectrum

The nonlinear matter power spectrum consists of two parts: the one halo term and the two halo term [15]. These are denoted as $P_{\rm 1h}$ and $P_{\rm 2h}$, respectively:

$$P(k) = P_{\rm 1h}(k) + P_{\rm 2h}(k)\,. \tag{3.7}$$

The one halo term is Fourier transform of the two-point correlation function for two points that are inside the same halo:

$$P^{\rm 1h}(k) = \int dM \frac{dn}{dM} \left(\frac{M}{\bar{\rho}}\right)^2 |u(k \mid M)|^2\,. \tag{3.8}$$

The one halo term depends only on the halo mass function and the halo density profile. The two halo term is the Fourier transform of the two-point correlation function for points that are in different halos:

$$\begin{aligned} P^{\rm 2h}(k) = & \int dM_1 \frac{dn}{dM_1} \frac{M_1}{\bar{\rho}} u(k \mid M_1) \\ & \times \int dM_2 \frac{dn}{dM_2} \frac{M_2}{\bar{\rho}} u(k \mid M_2) \\ & \times P_{\rm hh}(k \mid M_1, M_2)\,. \end{aligned} \tag{3.9}$$

[1] http://camb.info

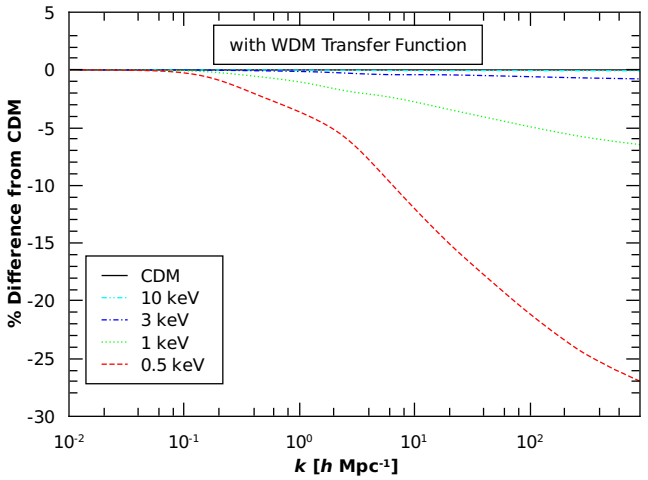

FIG. 2. Shown is the difference between the WDM models and CDM for the nonlinear matter power spectrum with only a change in the linear matter transfer function. The WDM particle masses are listed in the legend. This results in suppression of the power spectrum on small scales (large k) in the WDM models.

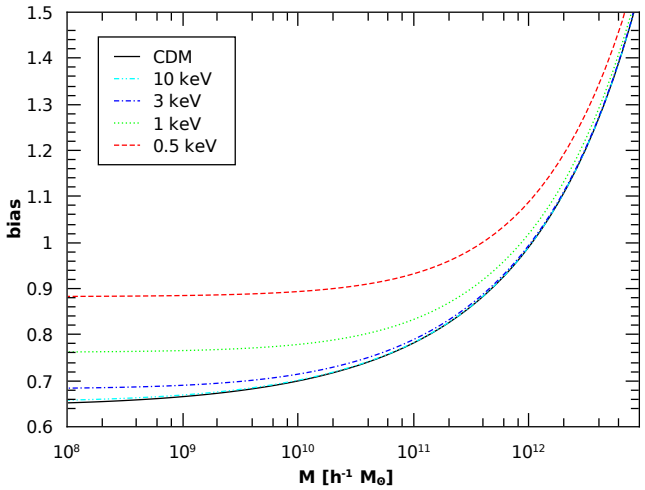

FIG. 3. Shown is the halo bias as a function of mass for CDM and several WDM particle masses, as given in the legend. The difference in the WDM models comes only from the change in $\sigma(M)$.

In addition to dependence on the mass and density functions, the two halo term also depends on the power spectrum of halos with masses M_1 and M_2 $(P_{\rm hh})$. $P_{\rm hh}$ can be approximated by the bias for each halo and the linear matter power spectrum:

$$P_{\rm hh}(k \mid M_1, M_2) \approx b_1(M_1)\, b_2(M_2)\, P_{\rm lin}(k). \qquad (3.10)$$

In the nonlinear matter power spectrum, the suppression of the linear matter power spectrum only directly effects the 2-halo term. As with the linear matter power spectrum, the nonlinear spectrum is suppressed at small scales, as shown in Fig. 2.

IV. HALO BIAS FUNCTION

The halo bias function describes how halos cluster relative to the matter power spectrum. It is defined as the ratio of the halo power spectrum to the linear power spectrum [37],

$$b^2(k) = \frac{P_{\rm hh}(k)}{P_{\rm lin}(k)}. \qquad (4.1)$$

As shown in Fig. 3, small mass halos are less strongly biased than higher mass halos. Ref. [38] showed that halos with $M < M_\star$ are more strongly clustered and halos with $M > M_\star$ are less strongly clustered than given from the bias function based on the standard Press-Schechter formalism [39]. $M_\star$ is the typical mass scale of halos that are currently collapsing. Ref. [40] also studied the halo bias function. They find that previous forms of the bias function overestimate the bias for halo masses slightly less than $M_\star$ and that the bias is approximately constant for small mass halos ($M < 0.1 M_\star$).

The halo bias function using a larger suite of simulations consistent with extended Press-Schechter formalism was found in Ref. [37], which we employ here. Specifically, we use the bias function in §3.1, Eq. (6):

$$b(\nu) = 1 - A\frac{\nu^a}{\nu^a + \delta_{\rm c}^a} + B\nu^b + C\nu^c \qquad (4.2)$$

with parameters given in Ref. [37], Table 2, where ν is defined by

$$\nu = \frac{\delta_{\rm c}}{\sigma(M)} \qquad (4.3)$$

where $\sigma(M)$ is the variance at a given mass scale.

The quantities $\delta_{\rm c}$ and $M_\star$ are defined in the spherical collapse model (see, e.g. Ref. [15]). Here, $M_\star(z)$ is defined as the typical mass that is collapsing at redshift z. The value for $M_\star$ is given by

$$\sigma(M_\star(z)) = \frac{\delta_{\rm c}}{D(z)}, \qquad (4.4)$$

where D is the linear growth, and note that $D(0) = 1$. The constant $\delta_{\rm c}$ is the density for collapse in the spherical collapse model, and is $\delta_{\rm c} = 1.69$.

In the case of WDM, $M_\star$ is not well-defined for all particle masses. For light masses, $\sigma(M)$ is less than $\delta_{\rm c}$ for all masses (see Fig. 4). This means that there are no typical halos that are currently collapsing. Since that is certainly not the case in the universe, these particle masses of WDM are not realistic.

The halo bias calculated from $\sigma(M)$ for the CDM model and several WDM particle masses is shown in Fig. 3. The bias is defined in terms of ν which, in turn, depends on $\sigma(M)$. Therefore, changes to the linear matter power spectrum also affect the bias function.

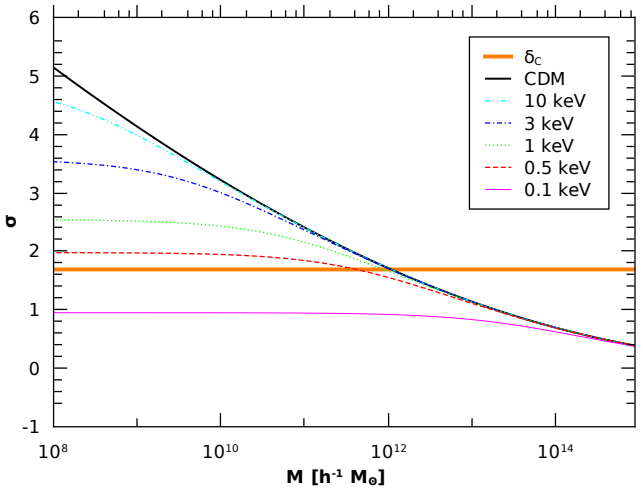

FIG. 4. Shown is $\sigma(M)$ for the CDM model and several WDM particle masses, as given in the legend. Here, M satisfying $\sigma(M) = \delta_c$ is the typical mass of halos which are currently collapsing. As shown, for very small WDM particle masses, such as 0.1 keV, typical fluctuation-scale halos have not collapsed, and little structure would have formed today.

Since the halo bias function has not been studied in WDM structure simulations, we use the bias function from Ref. [37] for both the CDM and WDM models. Though the halo bias should be tested in the case of WDM with simulations, it is beyond the scope of the present work.

V. HALO MASS FUNCTION

A. Cold Dark Matter

The halo mass function, dn/dM is the comoving number density of halos as a function of halo mass M and redshift z. From the spherical collapse model, overdensities in the matter density field must be at or above the critical density δ_c to collapse. (Recall the definition of $M_\star$ in equation (4.4).) The halo mass function can be estimated from the number of overdensities above the critical density. The following form was developed for the mass function, given Gaussian fluctuations in the initial density field:

$$\frac{m^2}{\bar{\rho}_z}\frac{dn}{dM}(M,z)\frac{dM}{M} = \nu f(\nu)\frac{d\nu}{\nu}. \tag{5.1}$$

The variable ν is defined in Eq. (4.3), and $\bar{\rho}_z$ is the average density of matter at redshift z. The function $f(\nu)$ is defined by

$$\nu f(\nu) = \sqrt{\frac{\nu}{2\pi}}\exp\left(-\frac{\nu}{2}\right). \tag{5.2}$$

The PS halo mass function is an approximation. Motivated by extensions to PS theory, numerical simulations find similar but more accurate relations for the halo mass function. We use the halo mass function from Ref. [41], Appendix C:

$$\frac{dn}{dM} = g(\sigma)\frac{\bar{\rho}_0}{M}\frac{d\ln\sigma^{-1}}{dM} \tag{5.3}$$

with $g(\sigma)$ defined as

$$g(\sigma) = B\left(\left(\frac{\sigma}{e}\right)^{-d} + \sigma^{-f}\right)\exp\left(-\frac{g}{\sigma^2}\right). \tag{5.4}$$

Their results for the constants B, d, e, f and g at several values of the mean interior density Δ are given in Ref. [41], Appendix C.

B. Warm Dark Matter

We find the halo mass function for CDM and three WDM particle masses in our simulations, described in §II. Our data shows that the suppression of the power spectrum on small scales, as expected, results in fewer low mass halos. We removed the upturn in number of halos with the smallest masses, which is a numerical artifact due to the discrete nature of the simulation [42]. We fit the WDM mass function as

$$\frac{dn'_{\rm W}}{dM} = \left(1+\frac{M_{\rm f}}{M}\right)^{-\eta}\frac{dn_{\rm C}}{dM}, \tag{5.5}$$

which does not include the erasure of the smallest scale halos. Here, $dn_{\rm C}/dM$ is the CDM mass function, and $M_{\rm f}$ is the filtering mass, which is defined as

$$M_{\rm f} = \frac{4\pi}{3}\bar{\rho}_0\frac{\pi^3}{k_{\rm f}^3} \tag{5.6}$$

where $k_{\rm f}$ is the wavenumber at which the WDM transfer function, Eq. (3.5), has an amplitude of 1/2. For sterile neutrinos with masses 0.5 keV, 1 keV, 3 keV and 10 keV, $k_f \approx 1.6$, 2.8, 7.3, and 20.5 hMpc^{-1}, respectively, and the filtering masses are $2.1\times10^{12}\ h^{-1}M_\odot$, $3.6\times10^{11}\ h^{-1}M_\odot$, $2.1\times10^{10}\ h^{-1}M_\odot$ and $9.8\times10^{8}\ h^{-1}M_\odot$ respectively. Eq. (5.5) is an accurate fit to the simulation's mass function for $\eta = 1.2$ (see Fig. 5).

Since the WDM particles free-stream out of the small scale perturbations, dark matter halo formation is strongly suppressed below the free-streaming scale $R_{\rm fs}$, which is defined as

$$R_{\rm fs} = 0.2\left(\Omega_{\rm dm}h^2\right)^{1/3}m_{\rm s}^{-4/3}. \tag{5.7}$$

This corresponds to a free-streaming scale mass $M_{\rm fs}$ at mean density (not to be confused with the filtering mass $M_{\rm f}$). We use this mass for our small scale cut-off in the mass function. We use an expression for the small halo suppression effect that is approximately unity when

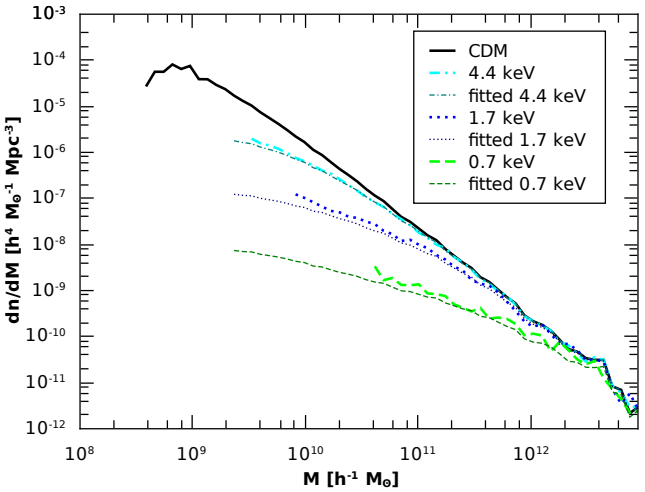

FIG. 5. Shown is the halo mass function from our simulations and our fits to that data. The thick lines are the data from each simulation, as listed in the legend. The thin lines are the CDM data multiplied by our fitting factor, which is given in Eq. (5.5).

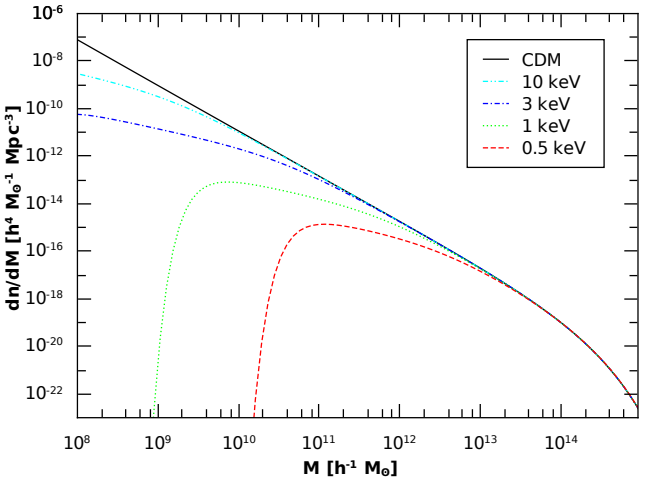

FIG. 6. Shown is the halo mass function for the CDM model and several WDM particle masses, as given in the legend. The mass functions are normalized to the CDM mass functions at large masses. Our WDM mass functions include a suppression for small M and a small scale cut-off.

$m \gg M_{\rm fs}$ and goes to zero when $m \ll M_{\rm fs}$ to provide a continuous cut-off. Our WDM mass function is then

$$\frac{dn_{\rm W}}{dM} = \left(\frac{M^2}{M^2 + M_{\rm fs}^2}\right)^{10^3} \left(1 + \frac{M_{\rm f}}{M}\right)^{-\eta} \frac{dn_{\rm C}}{dM}. \qquad (5.8)$$

The full mass function for our CDM and WDM models is shown in Fig. 6. The effect of just the change to the mass function on the nonlinear matter power spectrum is shown in Fig. 7. The decrease in small mass halos results in the suppression of the power spectrum at small scales.

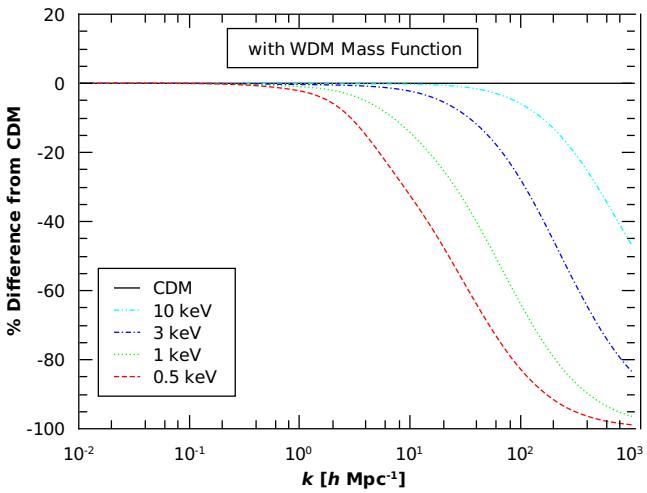

FIG. 7. The percent difference between the nonlinear matter power spectrum for the CDM model and several WDM particle masses, as listed in the legend, is plotted versus wavenumber k. In this graph, the only difference between the CDM and WDM models is the change to the mass function, as given in Eq.s (5.8). The decrease in small mass halos results in the suppression of the power spectrum at small scales.

VI. HALO DENSITY PROFILE

A. Cold Dark Matter

A general halo density profile is given by Ref. [43]:

$$\rho\left(r \mid M\right) = \frac{\rho_{\rm s}}{\left(\frac{r}{r_{\rm s}}\right)^{\gamma}\left[1 + \left(\frac{r}{r_{\rm s}}\right)^{\alpha}\right]^{(\beta-\gamma)/\alpha}}. \qquad (6.1)$$

For CDM, we employ the Navarro, Frenk and White (NFW) profile [44], which has $\alpha = 1$, $\beta = 3$ and $\gamma = 1$. The radius $r_{\rm s}$ is the radius at which the density function has a logarithmic slope of -2. For a spherically symmetric density profile, the mass of the halo is

$$M \equiv \int_0^{R_{\rm vir}} dr 4\pi r^2 \rho\left(r \mid M\right), \qquad (6.2)$$

for the virial radius $R_{\rm vir}$. For the NFW profile, the integral has an analytic solution, which specifies the value of $\rho_{\rm s}$:

$$M = 4\pi\rho_{\rm s} r_{\rm s}^3 \left(\ln\left(1+c\right) - \frac{c}{1+c}\right). \qquad (6.3)$$

The concentration c is defined as $c \equiv R_{\rm vir}/r_{\rm s}$. When calculating the nonlinear matter power spectrum, we use the Fourier transform of the density profile,

$$u\left(k \mid M\right) = \int_0^{R_{\rm vir}} dr 4\pi r^2 \frac{\sin\left(kr\right)}{kr} \frac{\rho\left(r \mid M\right)}{M}. \qquad (6.4)$$

B. Warm Dark Matter

The density profile of halos in WDM simulations has previously been studied by Avila-Reese and Colín et al. [43, 45, 46]. In [45], Milky Way size halos are simulated for WDM particles of mass 0.6, 1. and 2. keV. Ref. [45] found that the density profile of the halos is described by the NFW profile, but WDM halos can have an inner slope slightly shallower than −1. In Ref. [46], they simulate CDM and WDM halos with masses down to $0.01M_{\rm f}$. These halos were found to also be well described by the NFW profile. For WDM halos with masses below $M_{\rm f}$, it was found that the inner slope is shallower than in comparable CDM halos. In Ref. [43], halos with masses close to the filtering mass $M_{\rm f}$ were simulated, which found that the innermost ($r \lesssim 0.02R_{\rm vir}$) logarithmic slope of WDM halos is steeper than in the CDM model. Outside of this volume, the density profile for WDM halos is shallower than the NFW fit. Ref. [43] finds that, using the density profile of Eq. (6.1), a cored profile with $\alpha = 0.7$, $\beta = 3$ and $\gamma = 0$ fits the WDM halos. Ref. [23] uses a halo density profile where the size of the core increases as the mass of the halo decreases. The small mass halos $\left(M \lesssim 10^{11}\ h^{-1}M_{\odot}\right)$, in Ref. [23] have cores with radii on the order of $r_{\rm s}$. On the other hand, more recent work in Refs. [26, 27] studies whether WDM halos can have such cores, and shows that, in halo collapse modeling, the core of a WDM halo is smaller than $r \lesssim 10^{-3}R_{\rm vir}$. Below this scale, a core may need to be included in the density profile. Therefore, it is unlikely that WDM halos have large cores.

WDM halos that are smaller than the filtering mass (see Eq. (5.6)) have a shallower inner slope compared to CDM halos [45, 46]. Ref. [25] shows that, in CDM simulations, the slope of the inner profile depends on the effective spectral index $n_{\rm eff}$ of the initial power spectrum of the density perturbations at the scale of the power spectrum sampled by the halo $k_{\rm halo}$. That is, $P\left(k_{\rm halo}\right) \propto k_{\rm halo}^{n_{\rm eff}}$. Ref. [25] finds that

$$\gamma = \frac{9 + 3n_{\rm eff}}{5 + n_{\rm eff}}, \tag{6.5}$$

where γ is an exponent from Eq. (6.1). This is relevant to our WDM model since the suppression of the small-scale structure acts to decrease the effective spectral index at small scales, as in Fig. 1. This is what leads to a decrease in γ, the inner slope of the profile, though since $n_{\rm eff}$ is not well defined in WDM for a fixed halo mass, one cannot specify γ analytically.

We use our simulation of a $10^8\ M_{\odot}$ halo for CDM and three sterile neutrino WDM particle masses: 28 keV, 48 keV, and 70 keV. The density profile of these halos are shown in Fig. 8. We find that the simulated CDM and 70 keV WDM halos have an inner slope of −1.2. The inner slope of the simulated 48 keV WDM halo is −1.0, and the simulated 28 keV WDM halo has an inner slope of −0.8. We use an inner slope of −1 for the CDM cosmology,

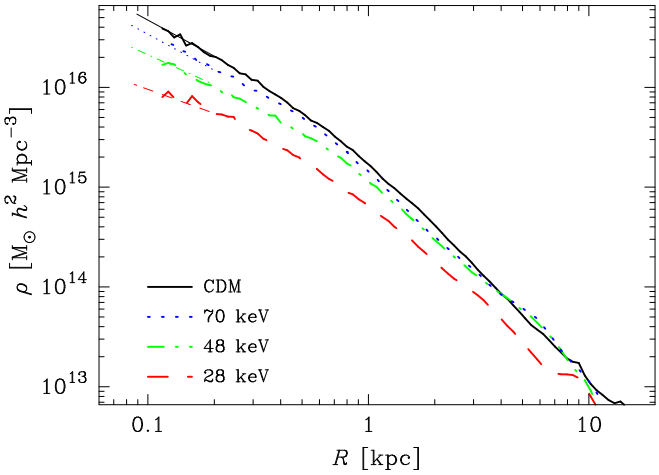

FIG. 8. This is a plot of the density versus radius for a $10^8 M_{\odot}$ halo simulated in four different WDM cosmologies, as given in the legend. The thick lines are data from the simulation, and thin lines show the estimated inner slope for the halo density profile, with $\gamma = 1.2$, $\gamma = 1.2$, $\gamma = 1.0$, $\gamma = 0.8$ for the CDM, 70 keV, 48 keV and 28 keV cases, respectively. The value γ describes the profile inner slope in Eq. (6.1).

as in the NFW profile. To model the effect of the suppression of the density profile, the inner slopes of halos composed of 70 keV, 48 keV, and 28 keV WDM particles are chosen to be −1, −0.8 and −0.6, respectively. We use these values to interpolate the inner slope for other WDM particle masses.

To include this effect, we make changes to the exponents in the profile density function (Eq. (6.1)). The exponent γ describes the logarithmic slope of the central section of the halo, where $r/r_{\rm s} \ll 1$. For the inner slope to be shallower, we use $\gamma < 1$. The smaller the mass of the WDM particle, the shallower the inner slope. When the inner slope of the density profile decreases, the density of the central region of the halo increases for a constant halo mass.

The exponent β describes the slope of the density profile for the outer edge of the halo, where $r/r_{\rm s} \gg 1$. The quantity α describes the sharpness of the change between the inner and outer sections of the density profile. For larger α, the changeover between a slope of γ and a slope of β is sharper. It takes place within a smaller region around $r/r_{\rm s} = 1$.

To maintain the definition of $r_{\rm s}$ as the radius at which the density profile has a logarithmic slope of −2, the exponents are constrained to be:

$$1 = \sqrt[\alpha]{\frac{\gamma - 2}{2 - \beta}} \Rightarrow \beta = 4 - \gamma. \tag{6.6}$$

Note that this relation is valid for $\alpha = 1$, $\beta = 3$ and $\gamma = 1$, which is the NFW profile.

Since the profile exponent change in γ changes the density distribution, in order to maintain a constant halo mass, the value of ρ_s must be rescaled with the pro-

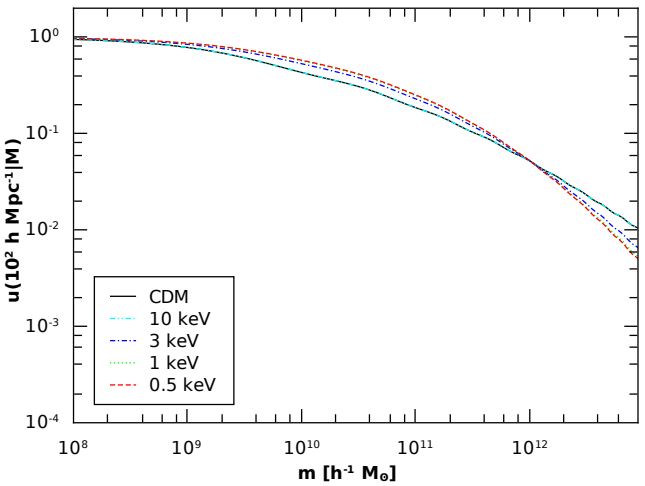

FIG. 9. The Fourier transform of the halo density profile $u\left(k|M\right)$ for a constant wavenumber of $10^2\ h^{-1}$Mpc is plotted as a function of halo mass M for the models listed in the legend.

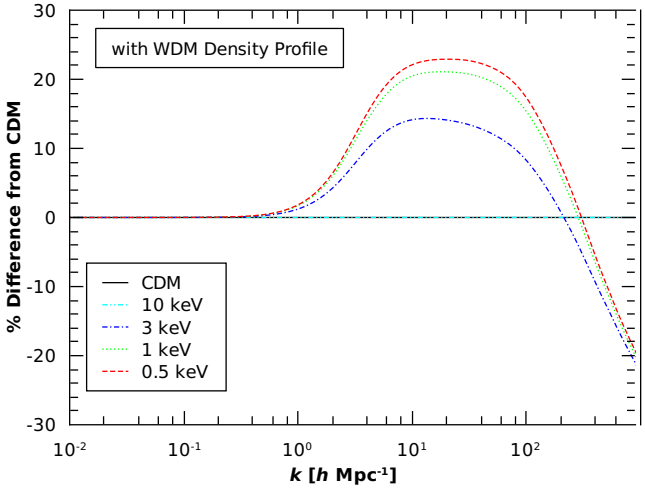

FIG. 10. The percent difference between the nonlinear matter power spectrum for the CDM model and several WDM particle masses, as listed in the legend, is plotted versus wavenumber k. In this graph, the only difference between the CDM and WDM models is the change to the inner slope of the halo density profile. The broadening of the central part of the halo and suppression of the peak results in a transfer of power from the smallest scales to slightly larger scales, as shown by the peak in the above plot.

file changes, which we incorporate in the WDM models. Shallower γ requires an increase in ρ_s, which broadens the density profile for a fixed halo mass. The Fourier transform of the density profile is employed in the nonlinear power spectrum. Fig. 9 is a plot of $u\left(k|M\right)$ for a constant wavenumber k. The increase in density around the halo center increases $u\left(k|M\right)$ for large k given a constant M. Fig. 10 shows the effect of changes to the halo density profile on the nonlinear matter power spectrum. The broadening of the central part of the halo and suppression of the central peak profile results in a transfer of power from the smallest scales to slightly larger scales, seen in Fig. 10.

VII. CONCENTRATION

The concentration of an NFW (see §VI) CDM halo has been found to be [24]

$$\bar{c}\left(m,z\right) \simeq \frac{9}{1+z}\left(\frac{m}{m_\star\left(z\right)}\right)^{-0.13}. \tag{7.1}$$

We apply the methodology described in Ref. [24] to the WDM linear power spectrum to determine the change in halo concentration.

The model in Ref. [24] is determined by two equations and the parameters F and K:

$$M_\star\left(z_{\rm c}\right) \equiv FM, \tag{7.2}$$

and

$$c\left(M,z_{\rm c}\right) = K\frac{1+z_{\rm c}}{1+z}, \tag{7.3}$$

where $M_\star$ is defined in Eq. (4.4).

We assume that $\sigma\left(M\right)$ is approximately a power law at a mass of $FM_\star$:

$$c \propto M^{-\alpha_c}. \tag{7.4}$$

Then, we can calculate α_c from $\sigma\left(M\right)$:

$$\alpha_c = \frac{d\left(\ln\sigma^{-1}\right)}{d\left(\ln M\right)} = \frac{-M}{\sigma}\frac{d\sigma}{dM}. \tag{7.5}$$

For the CDM case, the best fit parameters for F and$K$ are 0.01 and 4.0, respectively. Then, $\alpha_c = 0.13$, as in Eq. (7.1). This is valid for $0.01M_\star \lesssim M \lesssim 100M_\star$ [24]. Fig. 11 shows α_c as a function of WDM particle mass. The resulting concentration for halos in the CDM models and for several WDM masses is shown in Fig. 12. Since the exponent α_c decreases with WDM particle mass (see Fig. 11), the dependence of the concentration on halo mass also decreases. In addition, the concentration of halos in WDM models is less than in CDM [43, 45, 46].

Since α_c depends on the linear matter power spectrum through $\sigma\left(M\right)$, changing the concentration has an effect only if the linear matter power spectrum also changes. Fig. 13 shows the effect of the WDM linear matter power spectrum and concentration on the nonlinear matter power spectrum. The decrease in the concentration (see Fig. 12) increases the scale radius $r_{\rm s}$, from Eq. (6.1), which stretches the inner part of the halo profile relative to the radius. This also results in a transfer of power from the smallest scales to slightly larger scales, as shown by the peak in the nonlinear matter power spectrum.

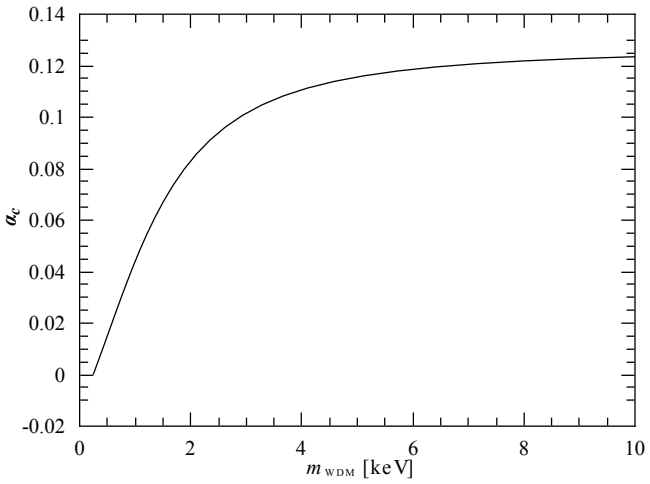

FIG. 11. The exponent in the concentration equation, Eq. (7.4), is plotted as a function of the WDM particle mass. As particle mass increases, α_c approaches 0.13, its value in the CDM model.

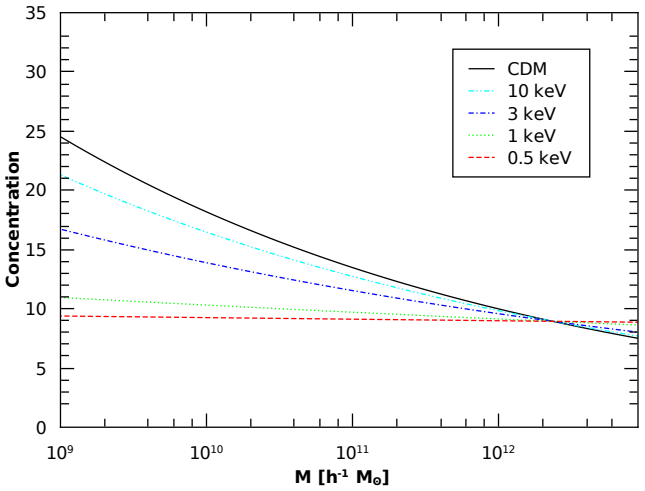

FIG. 12. The concentration of halos is plotted as a function of halo mass for the CDM model and several WDM particle masses, as given in the legend. Since the exponent α_c decreases with WDM particle mass (see Fig. 11), the dependence of the concentration on halo mass also decreases.

VIII. SUBSTRUCTURE

Clearly, in WDM, small mass halos are suppressed in number, and therefore subhalos will be suppressed as they are accreted halos in the hierarchical formation of large scale structure. Dolney et al. [47] study the effects of substructure on the CDM halo model. A halo consists of a smooth mass component and several subhalos. Most of the mass of the halo is in the smooth component. A fraction f of the mass is in the subhalos. Ref. [47] uses $f \approx 0.1$ and assumes that all subhalos are smaller than $0.01M$ where M is the mass of the host halo. With substructure, the one halo term becomes a sum of four

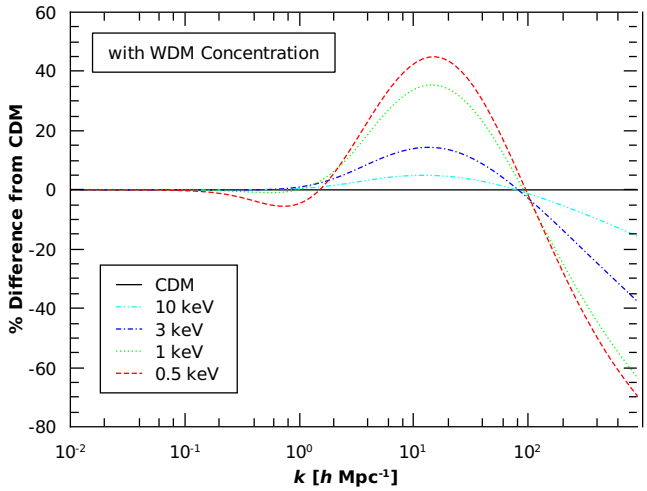

FIG. 13. The percent difference between the nonlinear matter power spectrum for the CDM model and several WDM particle masses, as listed in the legend, is plotted versus wavenumber k. In this graph, the WDM models differ from the CDM model in both the transfer function and concentration. The decrease in the concentration (see Fig. 12) increases the scale radius $r_{\rm s}$, from Eq. (6.1), which stretches the inner part of the halo profile relative to the radius. This results in a transfer of power from the smallest scales to slightly larger scales, as shown by the peak in the above plot.

different terms:

$$P_{\rm 1h} = P_{\rm ss} + P_{\rm sc} + P_{\rm 1c} + P_{\rm 2c}. \tag{8.1}$$

The first term in Eq. (8.1), $P_{\rm ss}$ describes correlations between two points of the smooth component of the host halo:

$$P_{\rm ss}(k) = \int dM \frac{dN}{dM} \left(\frac{M_{\rm s}}{\bar{\rho}}\right)^2 |U(k \mid M_{\rm s})|^2 . \tag{8.2}$$

Throughout this section, variables that are capital letters describe the host halo, and lower case variables are associated with the subhalos. Note the similarity of Eq. (8.1) to the one halo term without substructure, Eq. (3.8). The quantity $M_{\rm s}$ is the mass of the host halo that is in the smooth component ($M_{\rm s} = M(1-f)$), dN/dM is the mass function for host halos, and U is the density profile for host halos. The second term in Eq. (8.1) describes correlations between the smooth component of the host halo and the subhalos:

$$P_{\rm sc}(k) = 2 \int dM \frac{dN}{dM} \frac{M_{\rm s}}{\bar{\rho}} U(k \mid M_{\rm s}) U_{\rm c}(k \mid M_{\rm s}) \times \int dm \frac{dn}{dm} \frac{m}{\bar{\rho}} u(k \mid m) . \tag{8.3}$$

The expression $U_{\rm c}$ is the density profile for subhalos within the host halo, and dn/dm and u are the mass function and density profile for the subhalos. The third term from Eq. (8.1) is the correlation for two points within the

same subhalo:

$$P_{1c}(k) = \int dM \frac{dN}{dM} \times \int dm \frac{dn}{dm} \left(\frac{m}{\bar{\rho}}\right)^2 |u(k \mid m)|^2 . \quad (8.4)$$

The fourth term is the correlation between two different subhalos in the same host halo:

$$P^{2c}(k) = \int dM \frac{dN}{dM} |U_c(k \mid M_s)|^2 \times \left(\int dm \frac{dn}{dm} \frac{m}{\bar{\rho}} u(k \mid m) \right)^2 . \quad (8.5)$$

Dolney et al. [47] assume that the effect of substructure is negligible on the scale of correlations between two different halos, and we do the same. Therefore, the two halo term (Eq. (3.9)) remains the same.

The host halo mass function dN/dM and density profile U are as defined in the previous sections. For substructure, we need expressions for the spatial profile of subhalos within the host halo U_c, the mass function for subhalos dn/dm and the density profile with the subhalos u. We use the same density profile for the subhalos as for the host halos. The distribution of subhalos in the host halo is taken to be the density profile of the host halo U. The concentration for the subhalos is given by [24]:

$$\bar{c}(m, z) = \frac{7.5}{1+z} \left(\frac{m}{M_\star}\right)^{-0.30} . \quad (8.6)$$

The exponent -0.30 corresponds to $F \approx 200$ where F is taken from Eq. (7.2). The subhalo mass function is

$$\frac{dn}{dm}(M)\, dm = N_0 \left(\frac{M}{m}\right)^{\mu} \frac{dm}{m}. \quad (8.7)$$

The constant N_0 is determined by the fraction f of the halo mass in subhalos. This relation can be solved analytically to find

$$f = \int dm \frac{m}{M} \frac{dn}{dm}(M) = \frac{0.01^{(1-\mu)} N_0}{1-\mu}, \quad (8.8)$$

where the most massive subhalos are assumed to be one hundredth of the mass of the host halos. Dolney et al. [47] use a $\mu \approx 0.9$ for CDM.

A. Warm Dark Matter

In the CDM model, we employ the same density profile for halos and subhalos. When considering the effect of WDM on the subhalo density profile, we alter it in the same was as the halo density profile, which is described in §VI. Fig. 14 shows how changing the subhalo density profile with WDM particle mass affects the nonlinear matter power spectrum. In this figure, the CDM model also includes substructure. Since the center of the subhalo clumps shallower cusps, the smallest scales (highest k) transfer power to slightly larger scales. But, those scales also lose power to this effect, so the net result is negative.

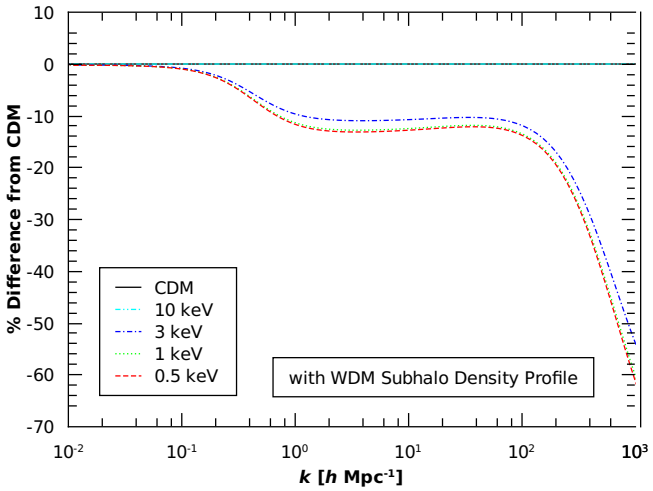

FIG. 14. The percent difference between the nonlinear matter power spectrum for the CDM model with substructure and several WDM particle masses, as listed in the legend, is plotted versus wavenumber k. In this graph, the WDM models differ from the CDM model in only the subhalo density profile. As with changes to the halo density profile, decreasing the inner slope of the subhalo density profile decreases the power on the smallest scales (large k).

For the subhalo concentration, we follow the procedure outlined in §VII, but use $F \approx 200$ where F is taken from Eq. (7.2). This allows us to calculate the exponent α_c, in Eq. (7.4), for the subhalo concentration. For the WDM particle masses 0.5 keV, 1 keV, 3 keV, and 10 keV, this exponent is 0.23, 0.25, 0.26, and 0.26, respectively. The effect of the subhalo concentration on the nonlinear matter power spectrum is shown in Fig. 15. The concentration of the subhalos decreases, which decreases the amplitude of the power spectrum on the smallest scales (large k).

For the subhalo mass function, we use our simulations to determine the change in the subhalo mass function relative to WDM particle mass. We want a function such that

$$\frac{dn_W}{dm} = g(m') \frac{dn_C}{dm}, \quad (8.9)$$

where $m' = m/M_f$ and M_f is the filtering mass. To find $g(m')$, we take the ratio of the WDM to CDM mass functions and change variables to m'. The result of this procedure for both the halo and subhalo mass functions is shown in Fig. 16. As expected from §V B, the halo mass function matches the multiplicative factor given in Eq. (5.5). That is,

$$\frac{dN_W/dM}{dN_C/dM} = \left(1 + M'^{-1}\right)^{-1.2}, \quad (8.10)$$

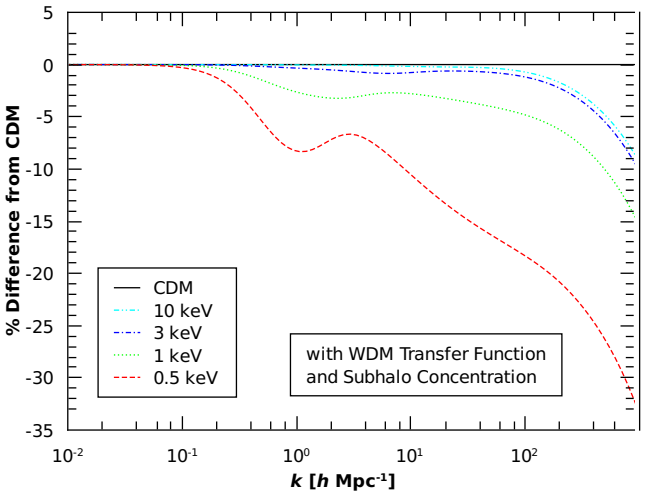

FIG. 15. The percent difference between the nonlinear matter power spectrum for the CDM model with substructure and several WDM particle masses, as listed in the legend, is plotted versus wavenumber k. In this graph, the WDM models differ from the CDM model in the transfer function and the subhalo concentration. The concentration of the subhalos decreases, which decreases the amplitude of the power spectrum on the smallest scales (large k).

where $M' = M/M_{\rm f}$ of the host halo. When the same procedure is applied to the subhalo mass function, we find that the data fits the same expression as for the halo mass function. As with the host halos, we use a small scale cutoff for the subhalos. Our subhalo mass function changes with WDM particle mass in exactly the same way as the halo mass function in Eq. (5.8), but using Eq. (8.7) for the CDM subhalo mass function. There may be slight evidence, as seen in Fig. 16, that the mass function for subhalos is less steep as a function of m'.

We normalize the subhalo mass function so that there are the same number of the largest subhalos (0.01 the halo mass) in CDM and WDM. The constant N_0 from Eq. (8.7) in the WDM model is related to CDM model by

$$N_{0\rm W} = \left(1 + 100\frac{M_{\rm f}}{M}\right)^{\eta} N_{0\rm C}. \tag{8.11}$$

The fraction of the halo mass in subhalos is determined by the integral in Eq. (8.8). Note the dependence on the host halo mass. The smaller the mass of the host halo, the smaller the fraction of the mass in subhalos.

The effect of the subhalo mass function on the nonlinear matter power spectrum is shown in Fig. 17. As the WDM particle mass decreases, the slope of the subhalo mass function μ decreases, and $M_{\rm fs}$ increases. This decreases the fraction of the host halo mass in subhalos and increases the fraction of the mass in the smooth component of the host halo. This is the reason for the increase in power in the nonlinear matter power spectrum between 0.1 and 1 h Mpc^{-1}. Power is transferred from the smallest scales, the subhalos, to somewhat larger scales, the host halo.

IX. SMOOTH BACKGROUND

The suppression of small mass halos results in some of the dark matter being in a smooth background component instead of collapsing into halos. The fraction of the dark matter in halos is:

$$f_{\rm h} = \frac{1}{\bar{\rho}_0}\int dM M\frac{dn}{dM}. \tag{9.1}$$

The fraction of the mass in halos is 0.95 for a 10 keV WDM particle, 0.76 for a 3 keV particle, 0.52 for a 1 keV particle and 0.36 for a 0.5 keV particle. We assume that the smooth component of the dark matter is related to the linear matter power spectrum by

$$b_{\rm s}^2 = \frac{P_{\rm ss}\left(k\right)}{P_{\rm lin}\left(k\right)}, \tag{9.2}$$

where $b_{\rm s}$ is derived in Ref. [23]:

$$b_{\rm s} = \frac{1 - f_{\rm h}b^{\rm eff}}{1 - f_{\rm h}}, \tag{9.3}$$

and $b^{\rm eff}$ is the effective mass weighted halo bias:

$$b^{\rm eff} = \frac{\int dM M\left(dn/dM\right)\ b\left(M\right)}{\int dM M\left(dn/dM\right)}. \tag{9.4}$$

The power spectrum for two points in the smooth component is [23]

$$P_{\rm ss}\left(k\right) = b_{\rm s}^2 P_{\rm lin}\left(k\right), \tag{9.5}$$

and the correlation between the smooth component and halos is

$$P_{\rm sh}\left(k\right) = \frac{b_{\rm s}P_{\rm lin}\left(k\right)}{\bar{\rho}_{\rm h}}\int dM\frac{dn}{dM}M\ u\left(k\mid M\right)\ b\left(M\right), \tag{9.6}$$

where $\bar{\rho}_{\rm h} = f_{\rm h}\bar{\rho}$. Then, the full power spectrum is:

$$\begin{aligned} P\left(k\right) = &\left(1 - f_{\rm h}\right)^2 P_{\rm ss}\left(k\right) \\ &+2\left(1 - f_{\rm h}\right) f_{\rm h} P_{\rm sh}\left(k\right) \\ &+P_{\rm 1h}\left(k\right) + P_{\rm 2h}\left(k\right). \end{aligned} \tag{9.7}$$

The full power spectrum and its components for a 0.7 keV WDM particle are shown in Fig. 18. Note that the smooth-smooth and smooth-halo terms are much smaller than the 2-halo term. Therefore, these terms should not significantly affect our results.

X. RESULTS

Fig. 19 is a graph of the percent difference of the nonlinear matter power spectrum in our WDM model with

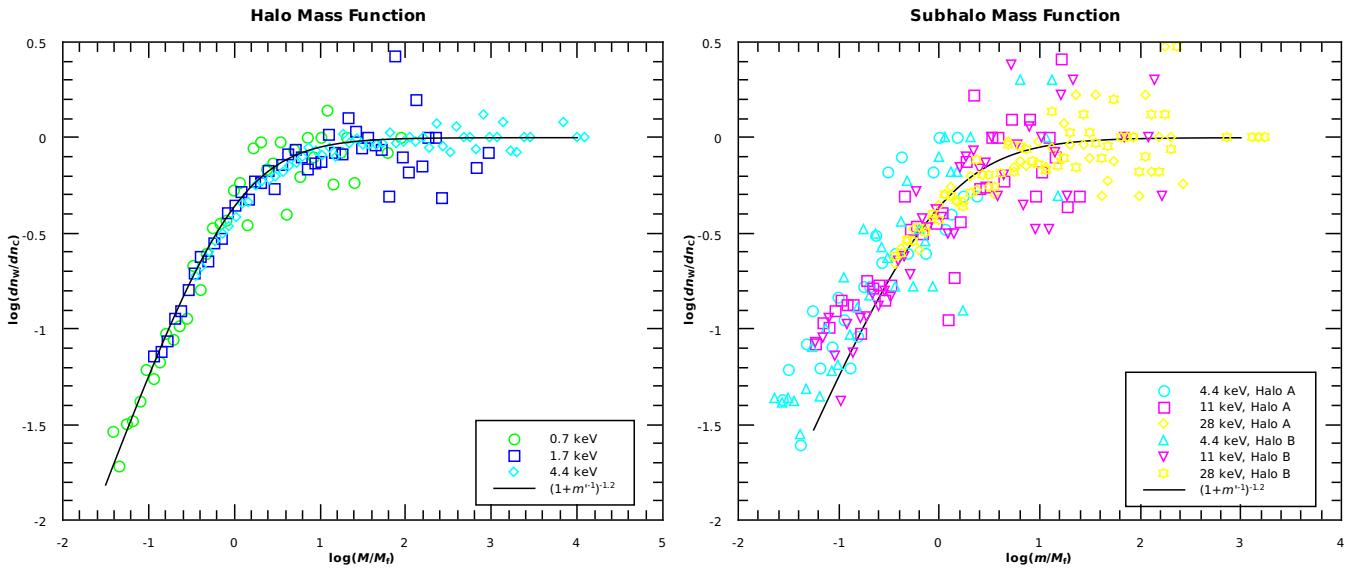

FIG. 16. The ratio of the WDM to CDM halo and subhalo mass functions from our set of simulations is plotted as a function of the halo or subhalo mass $m' = m/M_{\rm f}$ for several WDM particle masses, as given in the legends. The ratio of mass functions as a function of m' fits the same form, listed in the legend, for both the halo and subhalo mass functions.

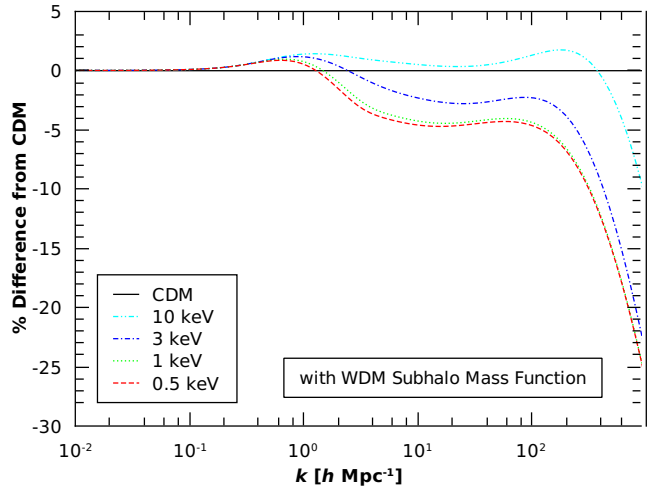

FIG. 17. The percent difference between the nonlinear matter power spectrum for the CDM model with substructure and several WDM particle masses, as listed in the legend, is plotted versus wavenumber k. In this graph, the WDM models differ from the CDM model in only the subhalo mass function. The changes to the subhalo mass function decrease the fraction of the host halo mass in subhalos and increase the fraction of the mass in the smooth component of the host halo. Power is transferred from the smallest scales, the subhalos, to somewhat larger scales, the host halo.

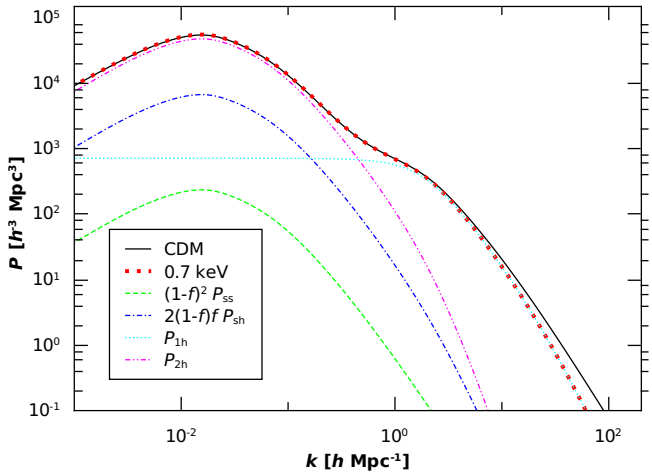

FIG. 18. The power spectrum for a 0.7 keV particle mass, is plotted versus wavenumber k. This graph includes the WDM mass function and the effect of a smooth background component to the dark matter. The smooth-smooth, smooth-halo, 1-halo and 2-halo power spectrums for a 0.7 keV WDM particle are also shown. Note that the smooth-smooth and smooth-halo terms are much smaller than the 2-halo term.

all effects except substructure. That is, the transfer function, mass function, halo density profile, and concentration are altered as described in the previous sections. At $k \approx 10h$ Mpc^{-1}, the strongest effects are from the concentration and halo density profile, which increase the power at these scales. All four of our alterations to the WDM model in this graph contribute to the decrease in power at small scales (large k).

Fig. 20 is a graph of the percent difference of the nonlinear matter power spectrum in our WDM model, including only the effects of WDM on the substructure and the transfer function, compared to the CDM model with substructure. The dominant effect at the 10 h Mpc^{-1} scale, especially for the 10 keV WDM particle, is from the subhalo mass function. For the 0.5 keV WDM par-

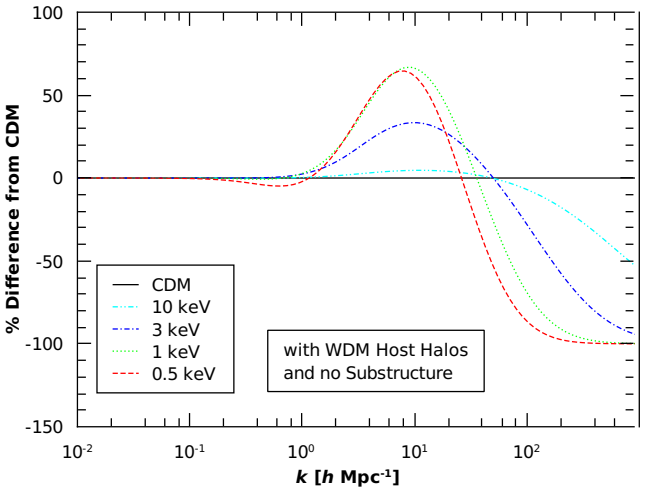

FIG. 19. The percent difference between the nonlinear matter power spectrum for the CDM model and several WDM particle masses, as listed in the legend, is plotted versus wavenumber k. This graph shows the results of changing the transfer function, mass function, halo density profile, and concentration. It does not include substructure. At $k \approx 10h$ Mpc^{-1}, the strongest effects are from the concentration and halo density profile, which increase the power at these scales. All four of our alterations to the WDM model in this graph contribute to the decrease in power at small scales (large k).

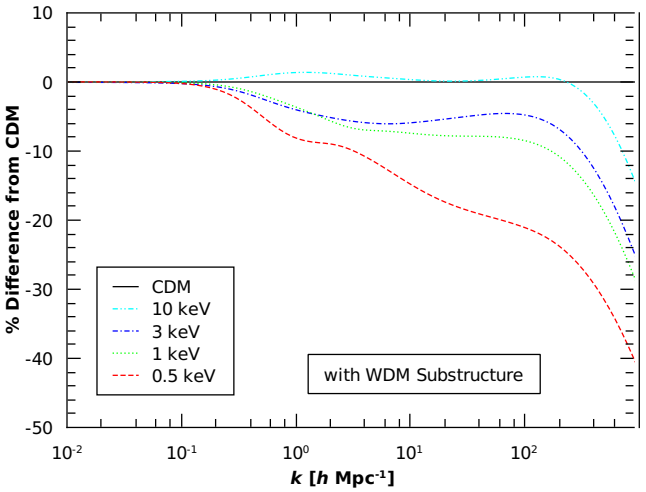

FIG. 20. The percent difference between the nonlinear matter power spectrum for the CDM model with substructure and several WDM particle masses, as listed in the legend, is plotted versus wavenumber k. This graph shows the results of changing the transfer function, the subhalo mass function, subhalo density profile, and subhalo concentration. The dominant effect here, especially for the 10 keV WDM particle, is from the subhalo density profile. For the 0.5 keV WDM particle, the largest effect is the decrease in power from the changes to the subhalo concentration.

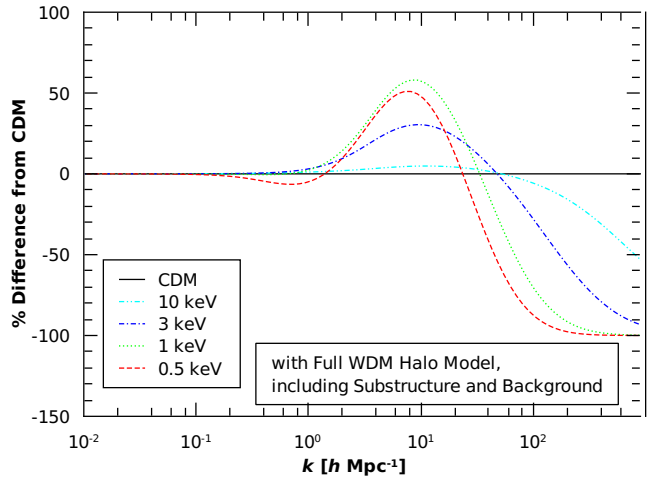

FIG. 21. The percent difference between the nonlinear matter power spectrum for the CDM model with substructure and several WDM particle masses, as listed in the legend, is plotted versus wavenumber k. This graph includes *all* of the adjustments to the WDM model detailed in this paper. This figure greatly resembles Fig. 19, with the increase in power at $k \approx 10h$ Mpc^{-1}. Therefore, the largest effects are from the changes to the host halo properties, with changes to the substructure and the addition of a smooth background component to the dark matter being sub-dominant.

ticle, the largest effect is the decrease in power from the changes to the subhalo concentration.

Fig. 21 is a graph of the percent difference of the nonlinear matter power spectrum for our WDM model with *all* of the effects discussed in this paper compared to the CDM model with substructure. The features in the changes of the nonlinear matter power spectrum greatly resemble those in Fig. 19. Therefore, the largest effects are from the changes to the main halo in WDM, with changes to the substructure and the addition of a smooth background component to the dark matter being smaller effects.

XI. CONCLUSION

We have presented our work on a broad assessment of the effects of WDM in the halo model of large-scale structure in two-point statistics, employing results from our own set of simulations as well as previously published work. This framework may be incorporated in a number of applications, including forecasts for large scale structure measures such as weak lensing [22, 23], in galaxy clustering two-point function measures of the power spectrum [48]. We have included the effects to the linear matter power spectrum, halo density profile, halo concentration relation, halo mass function, subhalo density profile, subhalo mass function and biasing of the smooth dark matter component in the case of WDM.

We find a drastic difference in the nonlinear matter

power spectrum predicted by the halo model between WDM and CDM even for reasonably "cold" WDM particle masses ($m_s = 10$ keV) at the smallest scales, as expected. We show that, counter-intuitively, WDM produces an enhancement of power at intermediate scales due to the softening of halo density concentrations and profiles. Since cored profiles are not found in WDM simulations, nor expected in analytic Gaussian peak statistics of WDM [26, 27], we do not include cored profiles, which differs our results from Ref. [23]. Also different from that work, we also include the effects of halo substructure, subhalo density profiles and subhalo mass functions. Ref. [22] only included the effects of the halo profile and halo mass function, and assumed all mass to be in halos, which is not the case in WDM.

We find that the host halo effects dominate the overall effects of WDM versus CDM in the nonlinear regime. Though our detailed results differ from previous work, the overall magnitude of the effects in the intermediate scale ($k \sim 10 - 100\ h\ \mathrm{Mpc}^{-1}$) regimes relevant for weak lensing are comparable, and therefore, the estimates for weak lensing sensitivity in that work are likely not drastically changed when incorporating our model in a weak lensing forecast.

The halo model has broad applications to observable cosmological statistics. With the help of the nonlinear structure framework of WDM versus CDM like that presented here, the observed large to small-scale clustering of matter, gas, and galaxies may be able to shed light on the nature of dark matter and its primordial origin.

ACKNOWLEDGMENTS

We would like to thank Manoj Kaplinghat for detailed comments on the manuscript and Anže Slosar for useful discussions. RMD and KNA are supported by NSF Grant 07-57966 and NSF CAREER Grant 09-55415. EP acknowledges support under the Edison Memorial Graduate Training Program at the Naval Research Laboratory.

[1] E. Komatsu *et al.* (WMAP Collaboration), Astrophys.J.Suppl. **192**, 18 (2011), arXiv:1001.4538 [astro-ph.CO].

[2] C. Burigana, C. Destri, H. de Vega, A. Gruppuso, N. Mandolesi, *et al.*, Astrophys.J. **724**, 588 (2010), arXiv:1003.6108 [astro-ph.CO].

[3] M. Kamionkowski and A. R. Liddle, Phys. Rev. Lett. **84**, 4525 (2000), astro-ph/9911103.

[4] K. Sigurdson and M. Kamionkowski, Phys. Rev. Lett. **92**, 171302 (2004), astro-ph/0311486; M. Kaplinghat, Phys. Rev. **D72**, 063510 (2005), astro-ph/0507300; J. A. R. Cembranos, J. L. Feng, A. Rajaraman, and F. Takayama, Phys. Rev. Lett. **95**, 181301 (2005), hep-ph/0507150CITATION = HEP-PH 0507150; .

[5] G. Kauffmann, S. D. M. White, and B. Guiderdoni, Mon. Not. Roy. Astron. Soc. **264**, 201 (1993); A. A. Klypin, A. V. Kravtsov, O. Valenzuela, and F. Prada, Astrophys. J. **522**, 82 (1999), astro-ph/9901240; B. Moore *et al.*, *ibid.* **524**, L19 (1999), astro-ph/9907411; B. Willman, F. Governato, J. Wadsley, and T. Quinn, Mon. Not. Roy. Astron. Soc. **353**, 639 (2004), astro-ph/0403001.

[6] P. J. E. Peebles, (2001), astro-ph/0101127.

[7] P. Bode, J. P. Ostriker, and N. Turok, Astrophys. J. **556**, 93 (2001), arXiv:astro-ph/0010389.

[8] J. J. Dalcanton and C. J. Hogan, Astrophys. J. **561**, 35 (2001), astro-ph/0004381; F. C. van den Bosch and R. A. Swaters, Mon. Not. Roy. Astron. Soc. **325**, 1017 (2001), astro-ph/0006048; A. R. Zentner and J. S. Bullock, Phys. Rev. **D66**, 043003 (2002), astro-ph/0205216; O. H. Parry, V. R. Eke, C. S. Frenk, and T. Okamoto, (2011), arXiv:1105.3474 [astro-ph.GA].

[9] A. D. Dolgov and J. Sommer-Larsen, Astrophys. J. **551**, 608 (2001).

[10] F. Governato *et al.*, Astrophys. J. **607**, 688 (2004), astro-ph/0207044; J. Kormendy and D. B. Fisher, Revista Mexicana de Astronomia y Astrofisica (Conference Series) **25**, 101 (2005), astro-ph/0507525.

[11] J. D. Simon and M. Geha, Astrophys.J. **670**, 313 (2007), arXiv:0706.0516 [astro-ph].

[12] E. Polisensky and M. Ricotti, Phys.Rev. **D83**, 043506 (2011), arXiv:1004.1459 [astro-ph.CO].

[13] U. Seljak, A. Makarov, P. McDonald, and H. Trac, Phys. Rev. Lett. **97**, 191303 (2006), arXiv:astro-ph/0602430; M. Viel *et al.*, Phys. Rev. Lett. **100**, 041304 (2008), arXiv:0709.0131 [astro-ph].

[14] M. Ricotti, N. Y. Gnedin, and J. Shull, Astrophys.J. **534**, 41 (2000), arXiv:astro-ph/9906413 [astro-ph]; J. Schaye, T. Theuns, M. Rauch, G. Efstathiou, and W. L. Sargent, Mon.Not.Roy.Astron.Soc. **318**, 817 (2000), arXiv:astro-ph/9912432 [astro-ph].

[15] A. Cooray and R. K. Sheth, Phys.Rept. **372**, 1 (2002), arXiv:astro-ph/0206508 [astro-ph].

[16] A. A. Berlind and D. H. Weinberg, Astrophys. J. **575**, 587 (2002), astro-ph/0109001.

[17] A. Cooray, W. Hu, and M. Tegmark, Astrophys.J. **540**, 1 (2000), arXiv:astro-ph/0002238 [astro-ph].

[18] R. K. Sheth, Mon.Not.Roy.Astron.Soc. **279**, 1310 (1996), arXiv:astro-ph/9511068 [astro-ph].

[19] A. Cooray, Mon.Not.Roy.Astron.Soc. **365**, 842 (2006), arXiv:astro-ph/0509033 [astro-ph].

[20] H. Zhan and L. Knox, Astrophys.J. **616**, L75 (2004), arXiv:astro-ph/0409198 [astro-ph]; D. H. Rudd, A. R. Zentner, and A. V. Kravtsov, Astrophys.J. **672**, 19 (2008), arXiv:astro-ph/0703741 [ASTRO-PH].

[21] K. Abazajian, E. R. Switzer, S. Dodelson, K. Heitmann, and S. Habib, Phys. Rev. **D71**, 043507 (2005), astro-ph/0411552CITATION = ASTRO-PH 0411552; ; S. Hannestad, H. Tu, and Y. Y. Wong, JCAP **0606**, 025 (2006), arXiv:astro-ph/0603019 [astro-ph].

[22] K. Markovic, S. Bridle, A. Slosar, and J. Weller, JCAP **1101**, 022 (2011), arXiv:1009.0218 [astro-ph.CO].

[23] R. E. Smith and K. Markovic, (2011), arXiv:1103.2134 [astro-ph.CO].

[24] J. S. Bullock, T. S. Kolatt, Y. Sigad, R. S. Somerville,

A. V. Kravtsov, *et al.*, Mon.Not.Roy.Astron.Soc. **321**, 559 (2001), arXiv:astro-ph/9908159 [astro-ph].
[25] M. Ricotti, Mon.Not.Roy.Astron.Soc. **344**, 1237 (2003), arXiv:astro-ph/0212146 [astro-ph].
[26] R. K. de Naray, G. D. Martinez, J. S. Bullock, and M. Kaplinghat, (2009), arXiv:0912.3518 [astro-ph.CO].
[27] F. Villaescusa-Navarro and N. Dalal, JCAP **1103**, 024 (2011), arXiv:1010.3008 [astro-ph.CO].
[28] H. Pagels and J. R. Primack, Phys.Rev.Lett. **48**, 223 (1982).
[29] S. Dodelson and L. M. Widrow, Phys. Rev. Lett. **72**, 17 (1994), hep-ph/9303287.
[30] D. N. Spergel, R. Bean, O. Doré, M. R. Nolta, C. L. Bennett, J. Dunkley, G. Hinshaw, N. Jarosik, E. Komatsu, L. Page, H. V. Peiris, L. Verde, M. Halpern, R. S. Hill, A. Kogut, M. Limon, S. S. Meyer, N. Odegard, G. S. Tucker, J. L. Weiland, E. Wollack, and E. L. Wright (WMAP Collaboration), Astrophys.J.Suppl. **170**, 377 (2007), arXiv:astro-ph/0603449 [astro-ph].
[31] V. Springel, Mon.Not.Roy.Astron.Soc. **364**, 1105 (2005), arXiv:astro-ph/0505010 [astro-ph].
[32] E. Bertschinger, Astrophys.J.Suppl. **137**, 1 (2001), arXiv:astro-ph/0103301 [astro-ph].
[33] S. R. Knollmann and A. Knebe, Astrophys.J.Suppl. **182**, 608 (2009), arXiv:0904.3662 [astro-ph.CO].
[34] M. Viel, J. Lesgourgues, M. G. Haehnelt, S. Matarrese, and A. Riotto, Phys. Rev. **D71**, 063534 (2005), astro-ph/0501562.
[35] D. J. Eisenstein and W. Hu, Astrophys.J. **511**, 5 (1997), arXiv:astro-ph/9710252 [astro-ph].
[36] K. Abazajian, Phys. Rev. **D73**, 063513 (2006), astro-ph/0512631.
[37] J. L. Tinker, B. E. Robertson, A. V. Kravtsov, A. Klypin, M. S. Warren, *et al.*, Astrophys.J. **724**, 878 (2010), arXiv:1001.3162 [astro-ph.CO].
[38] R. K. Sheth and G. Tormen, Mon.Not.Roy.Astron.Soc. **308**, 119 (1999), arXiv:astro-ph/9901122 [astro-ph].
[39] W. H. Press and P. Schechter, Astrophys.J. **187**, 425 (1974).
[40] U. Seljak and M. S. Warren, Mon.Not.Roy.Astron.Soc. (2004), arXiv:astro-ph/0403698 [astro-ph].
[41] J. L. Tinker, A. V. Kravtsov, A. Klypin, K. Abazajian, M. S. Warren, *et al.*, Astrophys.J. **688**, 709 (2008), arXiv:0803.2706 [astro-ph].
[42] J. Wang and S. D. M. White, (2007), arXiv:astro-ph/0702575.
[43] P. Colin, O. Valenzuela, and V. Avila-Reese, Astrophys. J. **673**, 203 (2008), arXiv:0709.4027 [astro-ph].
[44] J. F. Navarro, C. S. Frenk, and S. D. M. White, Astrophys. J. **462**, 563 (1996), astro-ph/9508025.
[45] P. Colin, V. Avila-Reese, and O. Valenzuela, Astrophys. J. **542**, 622 (2000), arXiv:astro-ph/0004115.
[46] V. Avila-Reese, P. Colin, O. Valenzuela, E. D'Onghia, and C. Firmani, Astrophys. J. **559**, 516 (2001), arXiv:astro-ph/0010525.
[47] D. Dolney, B. Jain, and M. Takada, Mon.Not.Roy.Astron.Soc. **352**, 1019 (2004), arXiv:astro-ph/0401089 [astro-ph].
[48] F. C. van den Bosch, H. Mo, and X. Yang, Mon.Not.Roy.Astron.Soc. **345**, 923 (2003), arXiv:astro-ph/0301104 [astro-ph]; K. Abazajian *et al.*, Astrophys. J. **625**, 613 (2005), astro-ph/0408003.